Proceedings of the
Annual Stability Conference
Structural Stability Research Council
Atlanta, Georgia, April 21-24, 2026

Local stability of 3D-printed stainless steel lipped angle sections under compression

Xi Chen[1], Jianing Cai[2], Guobin Gong[3], Yao Sun[4]

Abstract
Additive manufacturing, or 3D printing, is gaining increasing traction in structural engineering as a promising digital fabrication route. This study investigates the compressive behaviour of stainless steel lipped angle stub columns fabricated through the emerging wire-laser additive manufacturing technology (WLAM). Experimental work included compression tests on 16 WLAM lipped angle specimens, with results systematically compared against those of unlipped counterparts reported in prior research. The tests demonstrate that the lips significantly enhance the load-bearing capacity, with the strengthening effect being more pronounced in slender cross-sections. Thereafter, a detailed design analysis was conducted to evaluate the applicability of current European, American design standards, and the Continuous Strength Method, to WLAM stainless steel lipped angles. The findings indicate that existing international design codes yield inaccurate. By contrast, the Continuous Strength Method provides substantially improved predictive accuracy.

1. Introduction

The construction industry has increasingly adopted innovation and automation. A promising development in this regard is additive manufacturing (AM), often known as 3D printing, which has emerged as a transformative method in construction processes (Wu et al. 2016, Buchanan and Gardner 2019, Kühne et al. 2019). More recently, AM has been increasingly applied in structural engineering (Gardner 2023), by virtue of its distinct advantages relative to conventional methods. These benefits encompass enhanced design freedom, reduced material consumption, and lowered operational costs. Furthermore, AM enables the fabrication of complex geometries with improved structural performance—forms that are often difficult or economically infeasible to produce via conventional manufacturing techniques (Gardner 2023, Sun 2025). These advantages render AM particularly well-suited for engineering applications involving the use of stainless steel, a construction material characterised by superior mechanical performance and inherent corrosion resistance, yet its broader adoption is often constrained by its relatively high material cost (Gardner 2019, Sun and Zhao 2019, Ran et al. 2023a). Through design adaptability, AM enables the fabrication of material-efficient structural components, minimizing waste and lowering overall

[1] Postdoctoral Research Fellow, Hunan University, <xichen23@hnu.edu.cn>
[2] Research Assistant, Xi'an Jiaotong-Liverpool University, <jianing.cai21@student.xjtlu.edu.cn>
[3] Senior Associate Professor, Xi'an Jiaotong-Liverpool University, <guobin.gong@xjtlu.edu.cn>
[4] Full Professor, Hunan University, (corresponding author) <yaosun@hnu.edu.cn>

production costs (Chen and Sun 2025a, 2025b). Consequently, this capability mitigates the economic limitations traditionally associated with stainless steel, promotes the use in structural applications.

As a type of AM technology for metal 3D printing, wire-arc additive manufacturing (WAAM) employs an electric arc to melt and deposit wire feedstock incrementally. Extensive research has since been dedicated to elucidating the structural behaviour of WAAM-fabricated stainless steel components. Experimental investigations have examined various key aspects, including material properties (Kyvelou et al. 2020, Hadjipantelis et al. 2022, Zhao et al. 2023), cross-sectional behaviour (Kyvelou et al. 2021, Zhang et al. 2021, Evans et al. 2024, Chen et al. 2025), member stability (Weber et al. 2024), and connection performance (Guo et al. 2023, Meng et al. 2024, Liu et al. 2025). Despite these advances, key technical challenges impede the broader structural adoption of WAAM stainless steel, notably variability in mechanical properties, unpredictability of structural responses, and geometric imperfections such as distortion, humping, and surface roughness. In response to the inherent limitations of WAAM, a more advanced technique, wire-laser additive manufacturing (WLAM), has emerged as a promising alternative, which utilises a high-power laser beam as the heat source to melt steel wire feedstock. While both WAAM and WLAM are based on layer-by-layer wire deposition, WLAM is distinguished by its substantially higher energy density and smaller melt pool (Hong et al. 2025, Kyvelou et al. 2025). These features result in faster cooling rates and a superior surface finish compared to those achieved by WAAM. Moreover, WLAM can produce refined microstructures, leading to enhanced mechanical properties such as strength and fatigue resistance (Shim et al. 2025). Its high precision and material efficiency make WLAM particularly suitable for fabricating components with complex geometries and demanding performance requirements. The mechanical properties and microstructures of WLAM-fabricated austenitic stainless steel were studied (Xu et al. 2017), with the material found to exhibit satisfactory mechanical strength and a uniform microstructure. While such technological progress has been achieved, the structural performance and load-bearing capacity of WLAM stainless steel members remain inadequately investigated in the available literature.

To address this research gap, this paper presents an experimental investigation of the cross-sectional capacity of WLAM stainless steel stub columns with lipped angle sections. This study includes detailed fabrication procedures, material testing, geometry measurements, and a series of sixteen stub column tests using 316L stainless steel lipped angle sections. Subsequently, this study examines the suitability of established design standards prEN 1993-1-4 (2025), AISC 370 (2021) and the Continuous Strength Method (CSM) (Gardner et al. 2023) for the compression design of WLAM stainless steel lipped angles. The findings provide valuable insights into advancing the design and application of WLAM stainless steel in structural engineering.

2. Fabrication of Test Specimens

The WLAM stainless steel lipped angle sections used in this study were fabricated using a Laser-One 3D printer (Rongsu Technology, 2025). The sections were produced with six vortex laser beams as the power source and 1.2 mm diameter 316L austenitic stainless-steel wire as the feed material. The layers were printed perpendicular to the longitudinal axes of the angles. Two nominal material thicknesses – 3 and 5 mm – were adopted to evaluate thickness effects. To be specific, the robotic arm was programmed to move at travel speeds of 5 and 11 mm/s for fabricating angles with thicknesses of 3 and 5 mm, respectively. The corresponding wire feed rates of 10 and

14 mm/s were applied, which consistently produced layers with a height of 0.75 mm. Ultra-high-purity argon (99.998%) was used as a shielding gas at 13 L/min to prevent oxidation and maintain process stability (Rongsu Technology, 2025).

Based on the adopted WLAM process parameters, a total of 16 WLAM-fabricated stainless steel lipped angle stub columns were manufactured for compression testing. The cross-sectional profiles of these specimens were selected to account for variations in the geometric dimensions and plate slenderness ratios of the angle legs and lips, the data obtained via the following geometric measurements as summarized in Table 1. Specimens are labelled based on their leg width (b), plate thickness (t), and lip width (l_b), with lip thickness equal to leg thickness. The column length (L) was chosen as three times (Ziemian 2010) the leg width—a dimension long enough to incorporate representative imperfections yet short enough to suppress global buckling.

Table 1. Geometric dimensions of WLAM lipped angle stub columns.

Specimen ID	L (mm)	b (mm)	t (mm)	l_b (mm)	ω_l (mm)
L-40×3-5	119.4	39.6	2.97	5.10	0.12
L-45×3-5	134.2	45.2	2.95	5.07	0.13
L-50×3-5	150.4	51.0	2.99	4.88	0.13
L-60×3-5	178.9	60.5	3.03	5.11	0.15
L-60×3-10	180.1	60.4	2.98	9.86	0.20
L-70×3-5	211.1	72.3	3.05	5.14	0.22
L-80×3-5	238.7	79.4	3.04	5.02	0.18
L-90×3-5	269.5	92.1	3.05	5.11	0.25
L-40×5-5	118.6	39.4	4.92	5.05	0.11
L-45×5-5	134.2	44.2	4.95	5.25	0.15
L-50×5-5	150.2	50.9	4.89	5.12	0.14
L-50×5-10	150.6	49.8	4.91	10.01	0.14
L-60×5-5	179.6	62.3	4.87	5.27	0.21
L-70×5-5	210.7	71.1	4.99	4.90	0.23
L-80×5-5	239.2	79.2	4.91	4.95	0.19
L-90×5-5	270.5	89.1	4.89	5.02	0.18

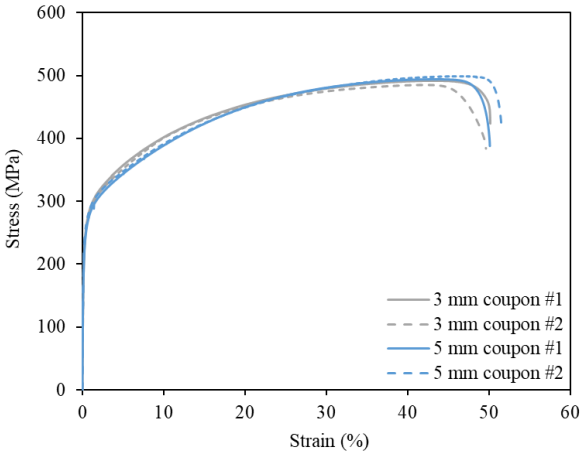

Figure. 1. Measured stress–strain histories (Sun and Chen 2025).

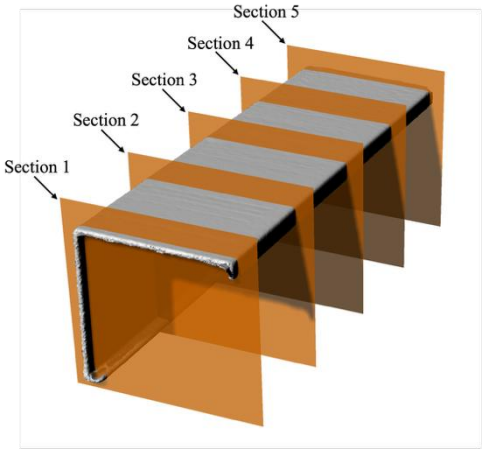

Figure 2. Cross-section extraction of scanned specimen L-90×3-5.

3. Testing Program and Experimental Results

Following the fabrication of WLAM stainless steel stub columns, a comprehensive experimental program was carried out to assess the cross-sectional behaviour and compressive capacity of these components. This program encompassed four material coupon tests, geometric property characterizations, and sixteen stub column compression tests.

3.1 Material Testing

The material properties of the WLAM stainless steel adopted have been carefully measured by the authors, following the measurement rig and detailed procedure in Sun and Chen (2025). To summarize, four tensile coupons from the same material batch as the columns were tested under monotonic loading following GB/T 228-1 (2021) in a 100 kN universal machine, with Digital Image Correlation (DIC) for strain measurement.

The stress–strain curves are shown in Fig. 1, while Table 2 reports the mechanical parameters, comprising ultimate strength (f_u), yield strength (f_y), fracture strain (ε_f), Young's modulus (E), ultimate-to-yield strength ratio (f_u/f_y) as well as hardening parameter (n). Both pairs of coupons display comparable stress-strain response profiles, suggesting that negligible discrepancies in mechanical behaviour arise between the two material thicknesses. Like conventional stainless steel (Ran et al. 2024a, 2024b), the WLAM material displays a rounded response with considerable strain hardening as corroborated by the high f_u/f_y ratios in Table 2.

Table 2. Mechanical properties of 316L stainless steel 3D-printed by WLAM.

Plate thickness (mm)	E (GPa)	f_y (MPa)	f_u (MPa)	f_u/f_y	ε_f (%)	n
3	191.2	247.2	488.4	2.0	50.4	5.1
5	193.6	241.4	496.4	2.1	51.1	5.6

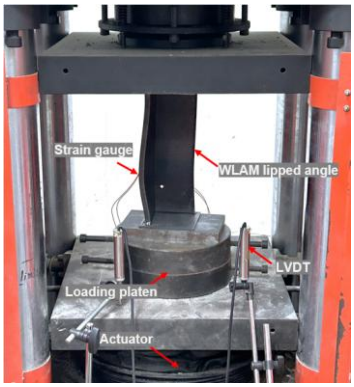

Figure 3. Stub column test setup.

3.2 Measurements of Geometric Properties

Geometric properties of the stub columns were measured using a Hexagon CMS 108 3D-laser scanner, with point cloud data processed into '.stl' models and visualised in Rhinoceros 3D. Cross-sectional dimensions and local imperfections were evaluated at five evenly spaced sections along each column length. Specifically, Section 1 and Section 5 were positioned 5 mm away from the two end sections of the specimen, while Section 2, Section 3 and Section 4 were taken at 0.25L, 0.5L, and 0.75L, as illustrated in Fig. 2 using the scanned stub column specimen L-90×3-5.

Measurements such as section width, plate thickness, and initial imperfections were derived from the data points to reveal geometric deviations caused by the additive manufacturing process. Centrelines for each cross-section were generated using linear regression on the measured point cloud data within MATLAB. For each section, the plate thickness t was computed as two times the mean perpendicular distance between the measured points and their respective fitted centrelines. Local imperfections were quantified by subtracting half the calculated plate thickness from the deviation between each point and the fitted centreline (Chen et al. 2025, Sun and Chen 2025). The final plate thickness for each WLAM lipped angle was given as the mean value across the five cross-sections, while the maximum deviation among them was used to represent the local imperfection (ω_l). Geometric dimensions for the WLAM stub columns are listed in Table 1.

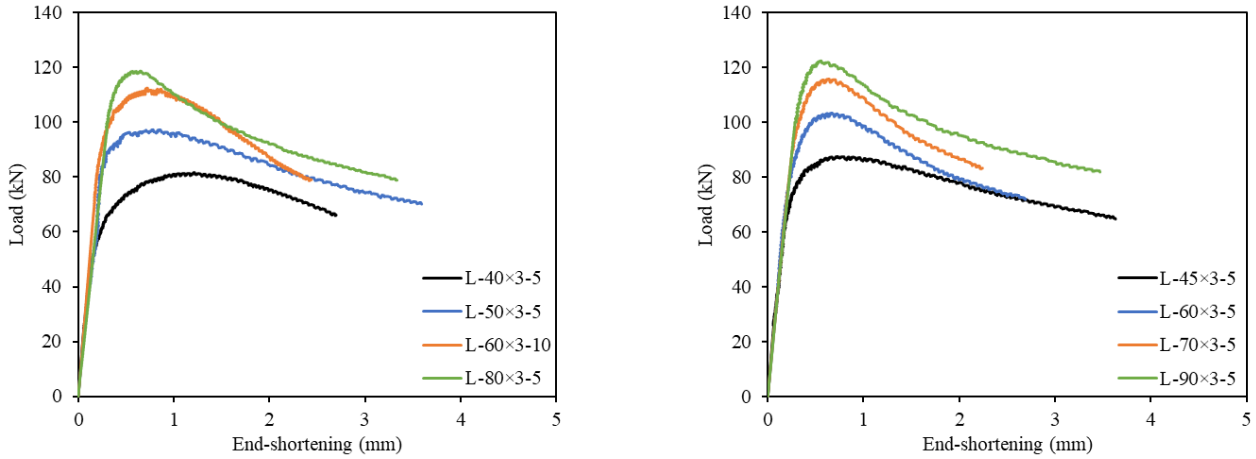

(a) 3-mm-thick WLAM lipped angle specimens.

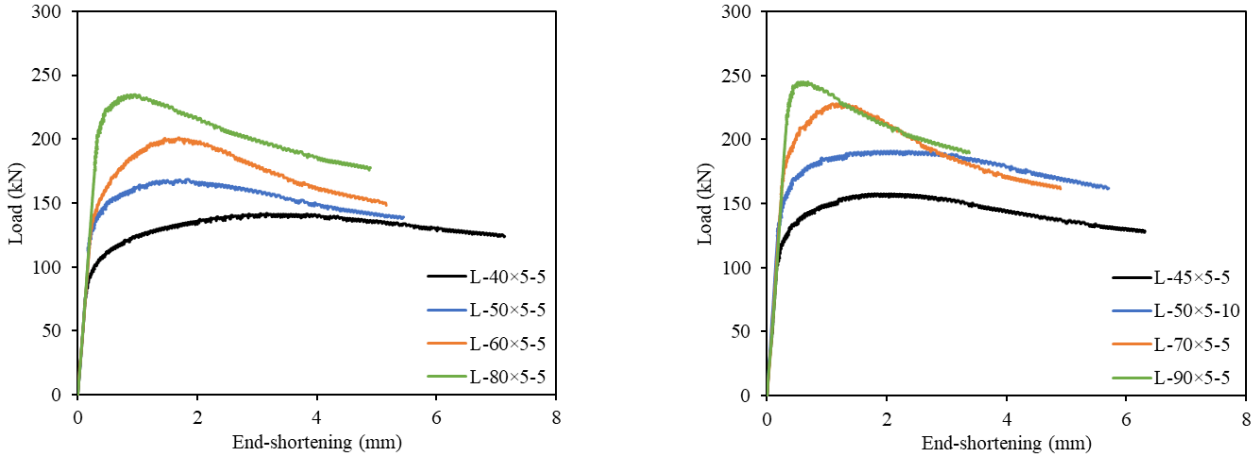

(b) 5-mm-thick WLAM lipped angle specimens.

Figure 4. Measured load–deformation curves.

3.3 Stub Column Tests

Stub column compression tests were performed on sixteen specimens to assess their cross-sectional compressive capacity. Prior to testing, both ends of each 3D-printed stub column were precisely machined to ensure flatness and parallel alignment and then welded with 4-mm-thick end plates, thereby promoting even stress distribution and fixed-ended boundary condition during loading. The test setup is illustrated in Fig. 3, which included two strain gauges and two LVDTs

to measure the axial strains at mid-height and the end-shortenings. A loading rate of 0.40 mm/min (Ran et al. 2023b) Sun and Chen 2025, Oluwadahunsi and Sun 2026, Yang and Sun 2026) was applied to each stub column ensuring consistent application of forces. The load–end-shortening behaviour of the stub columns across eight lipped angle section profiles is illustrated in Fig. 4, with key results presented in Table 3. During the initial stage of loading, the columns exhibited a linear load–deformation relationship with constant stiffness, indicative of elastic behaviour. As the load progressed, the curves showed a gradual reduction in slope, signifying a decrease in stiffness and the onset of localized deformation. The key results presented in Table 3 include ultimate loads (N_u), end-shortenings (δ_u), and ultimate-to-yield load ratios ($N_u/(Af_y)$), where A represents the gross cross-section area. Fig. 5 illustrates the failure mode observed in the tested stub columns, where significant localized deformation typically occurred near mid-height, matching the failure mode of conventional stainless steel stub columns (Yao et al. 2024, Young and Chen 2008, Young and Ellobody 2005).

(a) 3-mm-thick specimens. **(b)** 5-mm-thick specimens.

Figure 5. Failure mode of all tested WLAM lipped angle stub columns.

Table 3. Key stub column test results.

Specimen ID	N_u (kN)	δ_u (mm)	$N_u/(Af_y)$	$[N_{u,lipped}/(A_{lipped}f_y)]/[N_{u,unlipped}/(A_{unlipped}f_y)]$
L-40×3-5	81.7	1.78	1.29	1.22
L-45×3-5	87.4	2.06	1.23	1.23
L-50×3-5	97.4	2.36	1.21	1.25
L-60×3-5	103.3	2.11	1.08	1.35
L-60×3-10	112.5	1.78	1.11	1.37
L-70×3-5	115.6	1.94	1.01	1.38
L-80×3-5	118.7	2.24	0.95	1.53
L-90×3-5	122.3	2.15	0.85	1.44
L-40×5-5	142.0	4.12	1.42	1.08
L-45×5-5	157.7	3.32	1.40	1.11
L-50×5-5	168.5	3.47	1.33	1.11
L-50×5-10	183.0	2.98	1.35	1.10
L-60×5-5	201.1	2.69	1.31	1.14
L-70×5-5	228.1	2.78	1.29	1.15
L-80×5-5	234.9	2.67	1.21	1.23
L-90×5-5	245.1	2.31	1.13	1.27

Fig. 6 plots the ultimate-to-yield capacity ratio ($N_u/(Af_y)$) against the leg width-to-thickness ratio (b/t) for the tested specimens. The results show that larger b/t ratios correspond to

lower $N_u/(Af_y)$ ratios, indicating reduced cross-sectional structural efficiency for slenderer WLAM stainless steel lipped angles. Data points for the 3 and 5mm thick angles follow a highly similar trend, suggesting that material thickness has an insignificant effect on the normalized capacity and efficiency. A comparison is also made with unlipped WLAM angles of the same nominal dimensions tested in a previous study (Sun and Chen 2025). As seen in Fig. 6, the data points for the lipped angles consistently lie above those for the unlipped ones, demonstrating that the lips enhance the load-bearing capacity. This improvement is primarily due to the change in the supporting condition of the angle legs from outstand elements (one supported edge, one free) to internal elements (both edges supported). The strengthening effect of the lips becomes more pronounced as the b/t ratio increases. For angles with $b/t < 15$—classified as non-slender in prEN 1993-1-4 (2025) and having $N_u/(A_{fy}) > 1.0$—the capacity enhancement is relatively moderate. This is attributed to the fact that stockier stainless steel sections benefit more significantly from material strain hardening. In contrast, for angles with $b/t \geq 15$—classified as slender and having $N_u/(A_{fy}) \leqslant 1.0$—the capacity improvement is substantial. In this case, the lips effectively transform the slender outstand legs into non-slender internal elements, thereby increasing the cross-sectional efficiency.

The material utilization efficiency of lipped versus unlipped angles is further compared using the relative normalized compressive strength $[N_{u,lipped}/(A_{lipped}f_y)]/[N_{u,unlipped}/(A_{unlipped}f_y)]$, plotted in Fig. 7. All values exceed unity, reaffirming the capacity enhancement provided by the lips. This strengthening effect—and thus the material efficiency—increases with the b/t ratio, being more pronounced for slender sections. Quantitative results in Table 3 show the ratio ranges from 1.08 to 1.53, with mean values of 1.13 for non-slender angles ($b/t \leqslant 15$) and 1.34 for slender angles ($b/t > 15$). Additionally, for angles with different lip widths (e.g., L-50×5-5 vs. L-50×5-10), the normalized capacity shows negligible variation, indicating that increasing lip width does not necessarily improve cross-sectional efficiency.

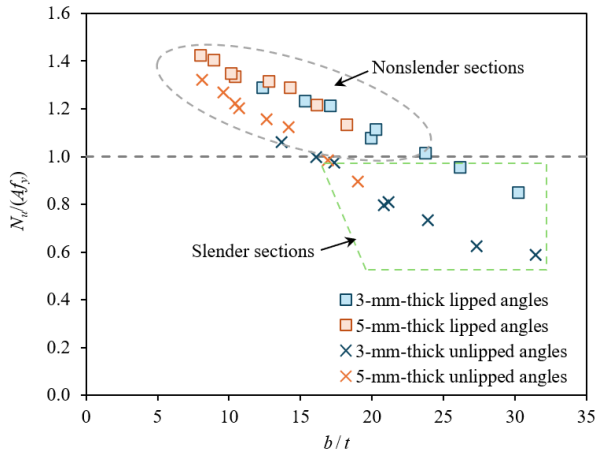

Figure 6. Comparison of normalized compressive capacities between WLAM stainless steel lipped and unlipped angles.

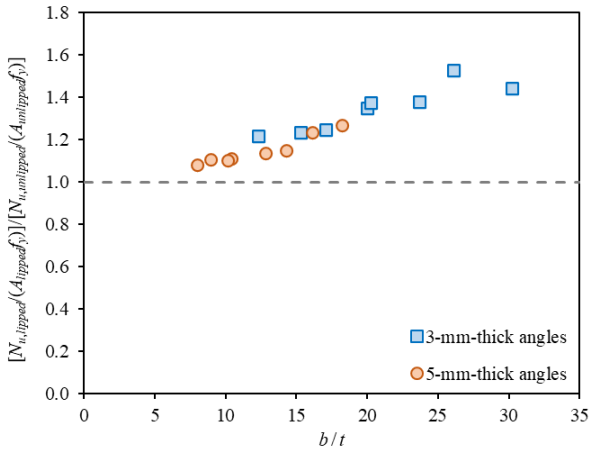

Figure 7. Relative normalized compressive strengths for WLAM angle sections.

4. Design Analysis

Following the experimental investigation, this section presents the corresponding design analysis. The design provisions of three international standards—prEN 1993-1-4 (2025), AISC 370 (2021), and the CSM (Gardner et al. 2023)—applicable to conventional stainless steel are summarized. Their applicability to WLAM lipped angles is subsequently validated against experimental test

data. The quantitative and graphical assessments for each approach are detailed in the following subsections. Table 4 summarize the mean test-to-predicted ultimate load ratios ($N_u/N_{u,pred}$) and coefficients of variation (CoVs) for each design method. These predicted values are given in the Table as $N_{u,EC3}$, $N_{u,AISC}$ and $N_{u,CSM}$, for prEN 1993-1-4 (2025), AISC 370-21 (2021) and the CSM (Gardner et al. 2023), respectively.

Table 4. Assessment of design approaches for WLAM lipped angles.

Design approaches	prEN 1993-1-4 $N_u/N_{u,EC3}$	AISC 370 $N_u/N_{u,AISC}$	CSM $N_u/N_{u,CSM}$
Mean	1.21	1.21	1.09
CoV	0.17	0.17	0.05

4.1 prEN 1993-1-4

For prEN 1993-1-4 (2025), the Eurocode classifies sections into slender (Class 4) or non-slender (Classes 1–3) based on plate width-to-thickness ratios relative to material parameters. Non-slender cross-sections can develop their nominal sectional yield strength Af_y, whilst slender sections fail before reaching Af_y due to elastic local instability. The classification is dependent on the constitutive lipped legs of the section, which are identified through the comparison between their width-to-thickness ratio $(b–2t)/t$ and the corresponding Class 3 slenderness limit, which is 35.4ε for compression elements with both edges supported, where $\varepsilon=(235/f_y)^{0.5}$ is the material parameter. Fig. 8 plots the Class 3 slenderness limit along with the $N_u/(Af_y)$ ratios, indicating that the Class 3 slenderness limit is not suitable for the classification of WLAM stainless steel lipped angles.

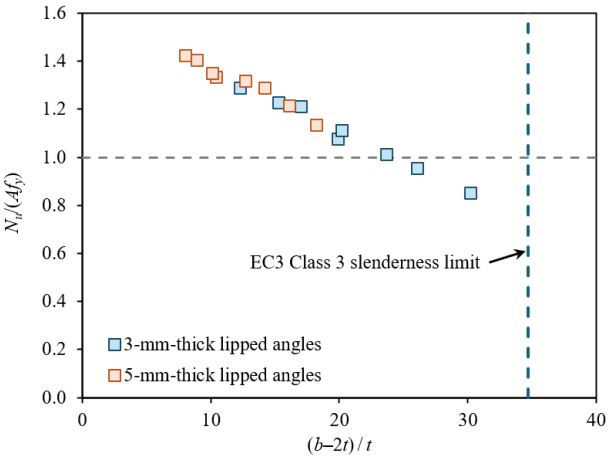

Figure 8. Evaluation of EC3 slenderness limit.

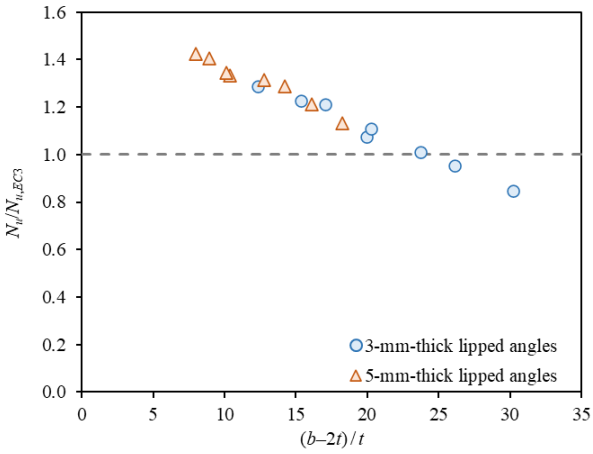

Figure 9. Evaluation of EC3-predicted capacities.

In terms of the design cross-sectional compressive capacity of lipped angles, the cross-sectional effective load ($A_{eff,EC3}f_y$) and yield load (Af_y) are used as the EC3-predicted capacity $N_{u,EC3}$ for slender and non-slender lipped angles, respectively, where $A_{eff,EC3}$ denotes the effective cross-sectional area according to EC3, calculated using the effective width method to account for elastic local buckling effects. The effective plate width can be determined by multiplying the original plate width and the reduction coefficient ρ_{EC3}, as expressed by Eq. (1), in which λ_p is the plate slenderness – see Eq. (2).

Based on the data, quantitative and graphical evaluations for WLAM stainless steel lipped angles were conducted, with the results summarized in Table 4. The mean value of the test-to-predicted

compressive capacity ratio ($N_u/N_{u,EC3}$) is 1.21, with a corresponding CoV of 0.17, indicating overall conservatism and scatter. As shown in Fig. 9, which plots the $N_u/N_{u,EC3}$ capacity ratios against the leg width-to-thickness ratios, the prEN 1993-1-4 (2025) provisions yield conservative predictions for stocky WLAM stainless steel lipped angles, primarily because the code neglects the beneficial effect of material strain hardening, which significantly enhances the capacity of such sections. Conversely, for slender sections, the code provides non-conservative (unsafe) over-predictions. This inaccuracy stems from an improper cross-section classification, which overestimates the effective area and consequently fails to adequately capture the local buckling resistance of slender profiles.

$$\rho_{EC3} = \frac{0.655\lambda_p - 0.012}{\lambda_p^{\,2}} \le 1 \tag{1}$$

$$\lambda_p = \frac{b/t}{55.4\varepsilon} \tag{2}$$

4.2 AISC 370

AISC 370 (2021) is the American specification established for stainless steel structures. In line with its European counterpart (2025), AISC 370 (2021) also utilises a cross-sectional classification framework to categorize thin-walled sections as slender and non-slender. For lipped angles, classification is made by comparing the lipped leg width-to-thickness ratio against predefined limiting value $1.24(E/f_y)^{0.5}$. The cross-sectional compressive capacity ($N_{u,AISC}$) is determined based on section classification: for non-slender sections, it is the yield capacity (Af_y); for slender sections, it is the effective sectional capacity ($A_{eff,AISC}f_y$). The effective area $A_{eff,AISC}$ is calculated using the effective width method, incorporating a reduction factor ρ_{AISC} (Eq. (3)). The elastic local buckling stress (f_{el}) required for ρ_{AISC} is obtained from Eq. (4).

$$\rho_{AISC} = 0.772\left(1 - 0.1\sqrt{\frac{f_{el}}{f_y}}\right)\sqrt{\frac{f_{el}}{f_y}} \le 1.0 \tag{3}$$

$$f_{el} = \frac{\pi^2 E}{3\left(1-0.3^2\right)}\left(\frac{t}{(b-2t)}\right)^2 \tag{4}$$

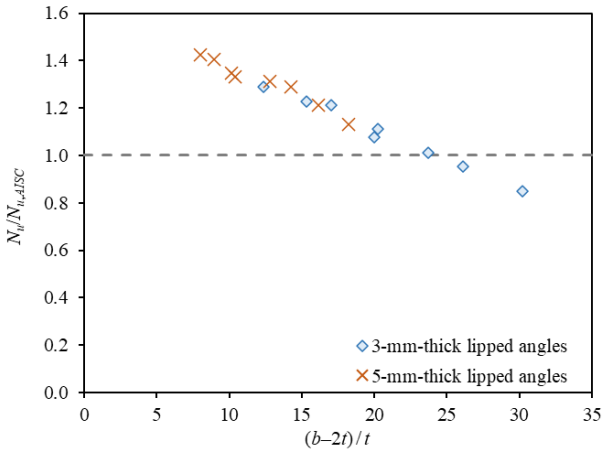

Figure 10. Evaluation of AISC-predicted capacities.

Fig. 10 plots the test-to-predicted capacity ratios ($N_{u,AISC}$) against width-thickness ratios. The results indicate that AISC 370 (2021) unduly underestimates the strength of stocky WLAM angles ($N_u/(Af_y) \geqslant 1.0$) while unsafely overestimating that of slender ones ($N_u/(Af_y) < 1.0$). As shown in Figs. 9 and 10, the evaluations for prEN 1993-1-4 (2025) and AISC 370 (2021) are nearly identical. This similarity stems from a common issue: the slenderness limits in both codes are unsuitable for classifying WLAM stainless steel lipped angles. Specifically, tested angles with $N_u/(Af_y) < 1.0$ (e.g., L-80×3-5 and L-90×3-5), which are in fact slender and cannot attain their full yield capacity, are misclassified as non-slender. Consequently, their design strength is incorrectly prescribed as Af_y rather than being reduced for local buckling. This renders the effective width equations in both codes inapplicable to these WLAM sections. For stocky angles with $N_u/(Af_y) \geqslant 1.0$, their capacity is underestimated primarily due to the neglect of material strain hardening in the design models.

4.3 CSM

The preceding evaluations indicate that existing design codes yield inaccurate capacity predictions for WLAM stainless steel lipped angle stub columns. These inaccuracies arise mainly from the neglect of strain hardening and the use of unsuitable cross-section classification limits and effective width formulations. In contrast, CSM (Gardner et al. 2023), which explicitly accounts for strain hardening and eliminates the need for cross-section classification, provides a more accurate predictive framework. The application of the CSM (Gardner et al. 2023) proceeds as follows: First, the CSM strain limit (ε_{csm}), which characterizes the cross-section's deformation capacity, is determined from the 'base curve' in Eq. (5). In this equation, the yield strain is $\varepsilon_y = f_y/E$, and the cross-section slenderness is $\lambda_s = (f_y/f_{cr,s})^{0.5}$, where $f_{cr,s}$ is the elastic local buckling stress obtained via finite strip analysis, for example GBTul (Bebiano et al. 2018). Following this, the compressive capacity ($N_{u,CSM}$) is calculated via Eq. (6), where the strain-hardening modulus (E_{sh}) is defined by Eq. (7) and the CSM ultimate strain is $\varepsilon_{u,csm} = 1 - f_y/f_u$.

$$\frac{\varepsilon_{csm}}{\varepsilon_y} = \begin{cases} \dfrac{0.25}{\lambda_s^{3.6}} \leq \min\left(15, \dfrac{0.1\varepsilon_{u,csm}}{\varepsilon_y}\right) & \text{for } \lambda_s \leq 0.68 \\ \left(1 - \dfrac{0.222}{\lambda_s^{1.05}}\right)\dfrac{1}{\lambda_s^{1.05}} & \text{for } \lambda_s > 0.68 \end{cases} \tag{5}$$

$$N_{u,CSM} = \begin{cases} Af_y \dfrac{\varepsilon_{csm}}{\varepsilon_y} & \text{for } \dfrac{\varepsilon_{csm}}{\varepsilon_y} \leq 1.0 \\ Af_y + AE_{sh}\varepsilon_y\left(\dfrac{\varepsilon_{csm}}{\varepsilon_y} - 1\right) & \text{for } \dfrac{\varepsilon_{csm}}{\varepsilon_y} > 1.0 \end{cases} \tag{6}$$

$$E_{sh} = \frac{f_u - f_y}{0.16\varepsilon_{u,csm} - \varepsilon_y} \tag{7}$$

Fig. 11 presents the test-to-predicted capacity ratios for the CSM (Gardner et al. 2023), demonstrating that its predictions closely align with the experimental results. This is supported by quantitative data in Table 4, where the mean ratio ($N_u/N_{u,CSM}$) is 1.09 with a CoV of 0.054 for the tested angles. Both graphical and quantitative assessments confirm that the CSM achieves substantially higher accuracy than the codified design guidelines for WLAM lipped angles in compression. The superior accuracy of the CSM is further illustrated in Fig. 12 through a direct comparison with the code-based predictions.

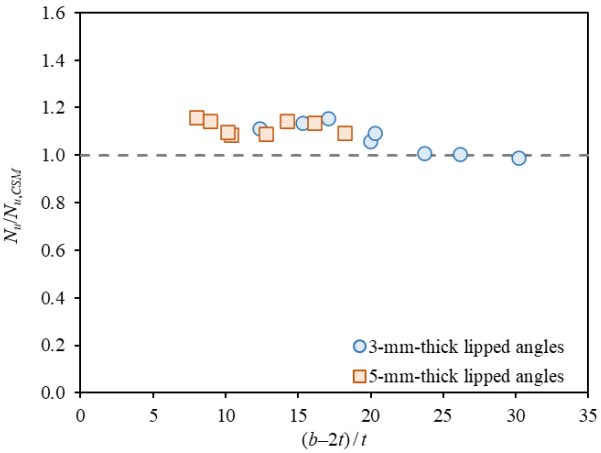

Figure 11. Evaluation of CSM-predicted capacities.

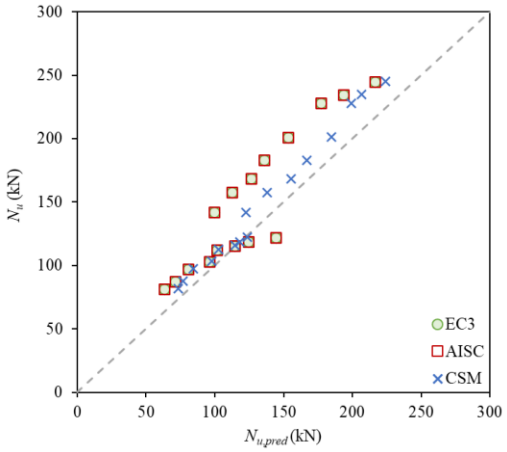

Figure 12. Comparison of design methods.

5. Conclusions

The cross-sectional compressive capacity and behaviour of WLAM stainless steel lipped angles have been systematically investigated in this study through experimental testing and design analysis. Sixteen stub column specimens, fabricated using the advanced WLAM technique, were tested under axial compression, all of which failed by local deformation. Based on the experimental results, the reinforcing effect of the lips on the cross-sectional compressive capacity was evaluated. The applicability of three design approaches – prEN 1993-1-4, AISC 370 and the CSM – to WLAM stainless steel lipped angles was then examined. The key findings of this research are summarised as follows:

(i) The lips significantly enhance the load-bearing capacity of WLAM stainless steel angles by altering the boundary conditions of the angle legs. This strengthening effect is generally more pronounced for slender angles with larger leg width-to-thickness ratios.
(ii) The cross-section classification limits stipulated in prEN 1993-1-4 and AISC 370 are unsuitable for WLAM stainless steel lipped angles. This misclassification results in unsafe (unconservative) capacity predictions for slender sections. Conversely, the capacity of stocky sections is excessively underestimated due to the neglect of material strain hardening in these design codes.
(iii) The CSM, which rationally accounts for strain hardening and eliminates the need for discrete cross-section classification, provides substantially more accurate capacity predictions than the current codified design guidelines.

Acknowledgments

This work is supported by Fundamental Research Funds for the Central Universities (No: 020100-531119200260) and Natural Science Foundation of Hunan Province (No.: 2025JJ60293).

References

AISC (2021). ANSI/AISC 370-21: Specification for structural stainless steel buildings, American Institute of Steel Construction (AISC).

Bebiano, R., Camotim, D., & Gonçalves, R. (2018). "GBTul 2.0– A second-generation code for the GBT-based buckling and vibration analysis of thin-walled members." *Thin-Walled Structures*, 124, 235-257.

Buchanan, C., & Gardner, L. (2019). "Metal 3D printing in construction: A review of methods, research, applications, opportunities and challenges." *Engineering Structures*, 180, 332-348.
Chen, X., Zhao, O., Xu, F., Zhi, J., & Sun, Y. (2025). "Cross-sectional capacity of wire arc additively manufactured stainless steel channel section stub columns." *Journal of Structural Engineering*, 151(6), 04025057.
Chen X. & Sun Y. (2025a). "Experimental investigation of mechanical properties of 3D-printed normal-strength and high-strength steels." *Journal of Constructional Steel Research*, 234, 109773.
Chen X. & Sun Y. (2025b) "In-fire behavior of wire-laser additively manufactured austenitic stainless steel." *Construction and Building Materials*, 493, 143304.
El-Sayegh, S., L. Romdhane and S. Manjikian (2020). "A critical review of 3D printing in construction: benefits, challenges, and risks." *Archives of Civil and Mechanical Engineering*, 20(2) 34.
Evans, S. I., Hadjipantelis, N., & Wang, J. (2024). "Stub column tests on wire arc additively manufactured equal-leg angle sections." *Engineering Structures*, 317, 118591.
Gardner, L. (2019). "Stability and design of stainless steel structures–Review and outlook." *Thin-Walled Structures*, 141, 208-216.
Gardner, L. (2023). "Metal additive manufacturing in structural engineering-review, advances, opportunities and outlook." *Structures*, 47, 2178-2193.
Gardner, L., Yun, X., & Walport, F. (2023). "The continuous strength method–Review and outlook." *Engineering Structures*, 275, 114924.
GB/T 228-1:2021. (2021). Metallic materials—Tensile testing—Part 1: Method of test at room temperature. Standardization Administration of China (SAC).
Guo, X., Kyvelou, P., Ye, J., Teh, L. H., & Gardner, L. (2023). "Experimental study of DED-arc additively manufactured steel double-lap shear bolted connections." *Engineering Structures*, 281, 115736.
Hadjipantelis, N., Weber, B., Buchanan, C., & Gardner, L. (2022). "Description of anisotropic material response of wire and arc additively manufactured thin-walled stainless steel elements." *Thin-Walled Structures*, 171, 108634.
Hong, W., Kyvelou, P., Zhang, R., & Gardner, L. (2025). "Mechanical testing and microstructural analysis of wire laser beam directed energy deposited steel plates." *Materials & Design*, 114141.
Kühne, R., Feldmann, M., Citarelli, S., Reisgen, U., Sharma, R., & Oster, L. (2019). "3D printing in steel construction with the automated Wire Arc Additive Manufacturing." *ce/papers*, 3(3-4), 577-583.
Kyvelou, P., Hong, W., Zhang, R., & Gardner, L. (2025). "Mechanical properties and microstructure of wire laser metal deposited austenitic stainless steel." *Materials & Design*, 250, 113558.
Kyvelou, P., Huang, C., Gardner, L., & Buchanan, C. (2021). "Structural testing and design of wire arc additively manufactured square hollow sections." *Journal of Structural Engineering*, 147(12), 04021218.
Kyvelou, P., Slack, H., Mountanou, D. D., Wadee, M. A., Britton, T. B., Buchanan, C., & Gardner, L. (2020). "Mechanical and microstructural testing of wire and arc additively manufactured sheet material." *Materials & Design*, 192, 108675.
Lange, J., T. Feucht and M. Erven (2020). "3D printing with steel." *Steel Construction*, 13(3) 144-153.
Liu, Y., Ye, J., He, J., Lu, H., Quan, G., Wang, Z., & Zhao, Y. (2025). "Testing and design of wire and arc additively manufactured steel double-shear bolted connections with thick plates." *Journal of Constructional Steel Research*, 224, 109069.
Meng, X., Zhi, J., Xu, F., & Gardner, L. (2024). "Novel hybrid sleeve connections between 3D printed and conventional tubular steel elements." *Engineering Structures*, 302, 117269.
Oluwadahunsi S.E. & Sun Y. (2026). "Testing and design of stainless-steel channel stub columns 3D-printed by wire-laser additive manufacturing (WLAM)." *Journal of Structural Engineering (ASCE)*, 152(2), 04025268.
prEN 1993-1-4. (2025). Eurocode 3: Design of steel structures — Part 1-4: General rules – supplementary rules for stainless steels. European Committee for Standardization (CEN), Brussels.
Ran H., Jian L., Ma Y. & Sun Y. (2023a). "Behavior of stainless-steel hot-rolled channel section beam-columns: Testing, modeling, and design." *Journal of Structural Engineering (ASCE)*, 149(2), 04022247.
Ran H., Chen Z., Ma Y., Di Sarno L. & Sun Y. (2023b). "Local stability of laser-welded stainless steel slender I-sections under combined loading." *Journal of Constructional Steel Research*, 200, 107649.
Ran H., Ma J., Chen X., Sun Y., Gkantou M. & McCrum D. (2024a). "Local stability of laser-welded stainless-steel T-section stub columns." *Journal of Structural Engineering (ASCE)*, 150(7), 04024062.
Ran H., Wang Y., Chen Z., Chen X. & Sun Y. (2024b). "Testing, modelling and design of laser-welded stainless steel slender I-section beam-column members under combined compression and major-axis bending." *Thin-Walled Structures*, 203, 112238.
Rongsu Technology. (2024). AMmake R1 series for 3D printing, https://www.rongsu.com/#/production/r1 (accessed 17 July 2025).

Shah, I. H., N. Hadjipantelis, L. Walter, R. J. Myers and L. Gardner (2023). "Environmental life cycle assessment of wire arc additively manufactured steel structural components." *Journal of Cleaner Production*, 389.

Shim, Y. R., Kim, J. K., Jo, D. H., Yang, H. P., Yoon, S. W., Yu, U. Y., & Jeon, J. B. (2025). "Microstructure and mechanical properties of wire laser additive manufactured deposits and their tungsten inert gas welds." *Materials*, 18(6), 1308.

Sun, Y., & Zhao, O. (2019). "Material response and local stability of high-chromium stainless steel welded I-sections." *Engineering structures*, 178, 212-226.

Sun, Y. (2025). "In-fire material properties of wire-arc additively manufactured 3D-printed structural aluminum alloys." *Construction and Building Materials*, 474, 140946.

Sun, Y., & Chen, X. (2025). "Testing and design of wire-laser additively manufactured (WLAM) stainless steel angle section stub columns." *Thin-Walled Structures*, 113351.

Weber, B., Meng, X., Zhang, R., Nitawaki, M., Sagawa, T., & Gardner, L. (2024). "Tensile behaviour of WAAM high strength steel material and members." *Materials & Design*, 237, 112517.

Wu, P., Wang, J., & Wang, X. (2016). "A critical review of the use of 3-D printing in the construction industry." *Automation in construction*, 68, 21-31.

Xu, X., Mi, G., Luo, Y., Jiang, P., Shao, X., & Wang, C. (2017). "Morphologies, microstructures, and mechanical properties of samples produced using laser metal deposition with 316 l stainless steel wire." *Optics and Lasers in Engineering*, 94, 1–11.

Yang P. & Sun Y. (2026). "Cross-sectional capacity of wire-laser additively manufactured (WLAM) high-strength steel angle stub columns." *Engineering Structures*, 348, 121748.

Yao, X., Ruan, C., Liu, Y., Liu, Y., Chen, H., Guo, Y., & Zeng, K. (2024). "Experiment and design of cold-formed steel equal-leg lipped angle under axial compression." *Results in Engineering*, 23, 102716.

Young, B., & Ellobody, E. (2005). "Buckling analysis of cold-formed steel lipped angle columns." *Journal of Structural Engineering*, 131(10), 1570-1579.

Young, B., & Chen, J. (2008). "Column tests of cold-formed steel non-symmetric lipped angle sections." *Journal of Constructional Steel Research*, 64(7-8), 808-815.

Zhang, R., Gardner, L., Buchanan, C., Matilainen, V. P., Piili, H., & Salminen, A. (2021). "Testing and analysis of additively manufactured stainless steel CHS in compression." *Thin-Walled Structures*, 159, 107270.

Zhao, Y., Chen, Y., Wang, Z., Ye, J., & Zhao, W. (2023). "Mechanical properties, microstructural characteristics and heat treatment effects of WAAM stainless steel plate material." *Journal of Building Engineering*, 75, 106988.

Ziemian, R. D. (2010). "Guide to stability design criteria for metal structures." John Wiley & Sons.